Sensors and Materials, Vol. 38, No. # (2026) 1–16
MYU Tokyo

S & M ####

Temporal Deep Learning Framework for Hysteresis Compensation in Carbon Nanotube–polydimethylsiloxane Soft Tactile Sensors

Nguyen Van Nghiem*†

Hanoi 10000, Vietnam

(Received April 30, 2026; accepted June 16, 2026)

Keywords: soft robotic sensors, hysteresis compensation, long short-term memory, deep learning, CNT–PDMS nanocomposite, tactile sensing

Piezoresistive soft tactile sensors based on carbon nanotube–polydimethylsiloxane (CNT–PDMS) nanocomposites have emerged as a pivotal technology for flexible electronics and soft robotics owing to their mechanical compliance and high sensitivity. However, their practical deployment remains significantly hindered by nonlinear and rate-dependent hysteresis, which arises from the viscoelastic nature of the elastomeric matrix and the dynamic reconfiguration of internal conductive networks. This path-dependent behavior introduces mapping ambiguity that degrades the reliability of real-time force estimation. Conventional compensation strategies, including phenomenological models such as the Prandtl–Ishlinskii approach, often require complex parameter identification and exhibit limited adaptability to varying dynamic conditions. In this study, a temporal deep learning framework utilizing a stacked long short-term memory network integrated with a sliding-window strategy is presented. Experimental validation on a 0.5 wt% CNT–PDMS sensor under cyclic loading (0.1–2.0 Hz) reveals a substantial reduction in maximum hysteresis error from 12.4 to 1.8% of the full-scale output. The proposed model, optimized via the Adam algorithm, achieves a coefficient of determination of 0.988, ensuring stable performance across diverse dynamic regimes. These findings demonstrate that temporal inference provides a robust and scalable solution for high-precision tactile perception in next-generation soft robotic platforms.

1. Introduction

Soft robotics has undergone rapid evolution in recent years, driven by the demand for systems capable of adaptive and safe interaction within unstructured environments.[1,2] A critical enabling component in these systems is an integration of compliant sensing technologies, widely known as electronic skins (e-skins), which provide real-time tactile feedback during physical interactions.[3,4] Among various transduction mechanisms, piezoresistive soft sensors based on conductive nanocomposites have attracted substantial interest owing to their structural simplicity, high mechanical compliance, and tunable electrical properties.[5,6]

*Corresponding author: e-mail: nghiemmsc@gmail.com
†Independent researcher
https://doi.org/10.18494/SAM6387

ISSN 0914-4935
https://myukk.org/

In particular, carbon nanotube–polydimethylsiloxane (CNT–PDMS) composites have emerged as a versatile material platform for tactile sensing and human–machine interfaces.[7,8] These sensors operate on the principle of deformation-induced variations in the internal conductive network, where changes in contact resistance and tunneling distance between nanotubes produce measurable variations in electrical resistance.[8,9] While these materials offer high sensitivity and stretchability,[6] their practical deployment is fundamentally constrained by nonlinear and rate-dependent hysteresis.[10] This phenomenon arises from the coupled effects of the viscoelastic relaxation of the PDMS matrix and the dynamic, irreversible reconfiguration of the conductive filler network during loading cycles.[11–13] Such path-dependence results in a multivalued mapping ambiguity, where a single resistance value may correspond to different force levels depending on the deformation history.[14,15]

The complexity of this hysteretic behavior is further exacerbated under dynamic conditions, as the area and shape of the hysteresis loop vary with the loading frequency.[10,12] Conventional calibration strategies typically rely on phenomenological models, such as the Prandtl–Ishlinskii (PI) and Duhem models.[12,15] Although these methods provide structured mathematical descriptions, they often necessitate complex, nonconvex parameter identification processes and exhibit limited adaptability to varying dynamic regimes or stochastic measurement noise.[2,16] Furthermore, while static machine learning models such as multilayer perceptrons (MLPs) can approximate global nonlinearities, they treat each measurement as an independent event, failing to capture the temporal context required to resolve memory-dependent hysteresis.[17]

Recent advancements in tactile intelligence suggest that temporal deep learning offers a superior framework for modeling complex sensor dynamics.[4,18] Recurrent architectures, specifically long short-term memory (LSTM) networks, are designed to process sequential data by incorporating internal gating mechanisms that retain relevant historical information.[19] By formulating hysteresis compensation as a temporal inference problem, it becomes possible to decode the deformation history and reconstruct a single-valued, linearized force relationship.[17,19] Despite the potential of these architectures, a unified framework that explicitly addresses both rate-dependence and hierarchical feature extraction in CNT–PDMS systems remains limited.[2]

In this work, we propose a temporal deep learning framework based on a stacked LSTM network integrated with a sliding-window strategy for hysteresis compensation in CNT–PDMS soft tactile sensors.[16] The proposed architecture captures the hierarchical temporal features of the sensing signal, providing a linearized force output that is robust across a frequency range of 0.1–2.0 Hz. The model parameters were optimized using the Adaptive Moment Estimation (ADAM) algorithm[20] to ensure stable convergence and high estimation accuracy. The remainder of this paper is organized as follows: in Sect. 2, the fabrication process and modeling methodology are described in detail; in Sect. 3, the experimental results and comparative analysis are presented; and the conclusion of this study is given in Sect. 4.

2. Data, Materials, and Methods

2.1 Fabrication of CNT–PDMS soft tactile sensor

The electromechanical efficacy of piezoresistive soft sensors is fundamentally determined by the topological stability and formation of conductive networks within the elastomeric matrix.[5,13] In CNT–PDMS composites, this percolated network is highly sensitive to processing parameters, particularly the quality of filler dispersion and the polymer cross-linking kinetics.[3,8]

Initially, multiwalled carbon nanotubes (MWCNTs, commercial grade, >95% purity) with a high aspect ratio (>500) were dispersed in heptane at a concentration of 0.5 wt% using probe ultrasonication for 60 min.[5,7] This ultrasonic treatment is critical for overcoming the strong van der Waals attractions that induce CNT agglomeration, thereby promoting a uniform conductive framework throughout the composite. Subsequent to dispersion, the PDMS base and curing agent (Sylgard 184, Dow Corning) were introduced at a weight ratio of 10:1 and integrated into the CNT suspension.[3,13]

To ensure a homogeneous distribution of nanotubes and to eliminate structural defects that could impair signal reliability, the mixture was subjected to intensive mechanical stirring for 30 min followed by vacuum degassing for 1 h to remove trapped air bubbles.[8,13] The resulting composite was cast into standardized molds (30 × 30 × 5 mm^3) and thermally cured at 80 °C for 3 h.[3] This curing protocol facilitates the formation of a stable, percolated conductive network necessary for resolving complex tactile stimuli.[2,14] The finalized sensor exhibits a Young's modulus of 1.85 MPa and an initial conductivity of 0.12 S/m, aligning with the compliance requirements for safe human–machine interaction. Young's modulus was determined from uniaxial compression tests on the cured specimens, taken as the slope of the linear region (≤10% strain) of the stress–strain curve, while the initial conductivity was obtained from the steady-state resistance of the unloaded sensor measured by a four-point probe together with the specimen geometry.[6,18] The key material properties and experimental parameters are summarized in Table 1.

Table 1
Technical specifications of CNT–PDMS sensor and experimental system.

Category	Parameter	Symbol/model	Value	Unit
Material	Base elastomer	PDMS	Sylgard 184 (10:1)	—
	Conductive filler	MWCNTs	>95% purity	—
	Filler concentration	ω_c	0.5	wt%
Geometry	Sensor dimensions	$L \times W \times H$	30 × 30 × 5	mm
	Active area	A	900	mm^2
Physical properties	Young's modulus	E	1.85	MPa
	Initial conductivity	σ_0	0.12	S/m
Hardware	Load cell	—	Futek LSB200 (50 N, 0.1%)	—
	Data acquisition	—	NI USB-6009 (14-bit)	—
	Sampling frequency	f_s	100	Hz
	Linear actuator	—	Thorlabs LTS150	—

2.2 Experimental setup and data acquisition

To accurately characterize the dynamic electromechanical behavior of the CNT–PDMS sensor and establish a high-fidelity dataset for temporal modeling, a synchronized measurement platform was developed.[8,14] The experimental setup, designed to capture the instantaneous relationship between mechanical stress and electrical response, is illustrated in Fig. 1.

Mechanical stimuli were applied using a high-precision linear actuator (Thorlabs LTS150), which provided cyclic compressive displacements with a resolution of 0.1 μm. The reference force F_{ref}, serving as the ground-truth labels for the stacked LSTM model, was monitored using a calibrated load cell (Futek LSB200, 50 N capacity, 0.1% accuracy).[15,18] Prior to data acquisition, the load cell was calibrated using standard weights to ensure measurement traceability.[7]

The electrical resistance variation (ΔR) of the CNT–PDMS sensor was converted into a voltage signal using a Wheatstone bridge configuration integrated with an instrumentation amplifier. This hardware approach is essential for maximizing measurement sensitivity to subtle tunneling resistance changes and for suppressing common-mode noise inherent in nanocomposite systems.[3,9] Both force and resistance channels were digitized simultaneously using a 14-bit data acquisition system (NI USB-6009) at a sampling frequency f_s of 100 Hz. To ensure temporal consistency, all signals were sampled using a shared hardware clock.[17,20]

To enhance signal quality, a digital low-pass Butterworth filter was applied to suppress high-frequency environmental interference while preserving the low-frequency dynamics associated with viscoelastic relaxation and rate-dependent hysteresis.[12,13] The cutoff frequency f_c = 10 Hz (a fourth-order Butterworth filter) was strategically selected to avoid the phase distortion of the primary sensing signal, i.e., kept well above the highest mechanical excitation frequency of 2.0 Hz while attenuating high-frequency environmental noise. The resulting synchronized dataset was partitioned into training and testing subsets for the subsequent development of the temporal deep learning framework.

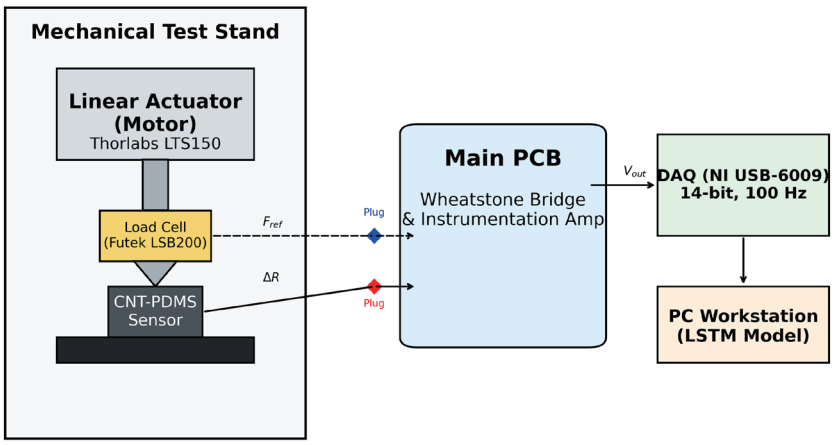

Fig. 1. (Color online) Experimental setup including linear actuator, reference load cell, CNT–PDMS sensor, signal conditioning circuit, and data acquisition system.

2.3 Stacked LSTM architecture

The synchronized dataset obtained from the experimental setup is used to train a temporal model for hysteresis compensation. As discussed in Sect. 2.2, the sensor response exhibits strong path dependence and rate dependence, indicating that the current output is intrinsically linked to its deformation history.[10,12] Traditional memoryless models fail to capture this evolution, necessitating a temporal modeling approach.[16] Consequently, a stacked LSTM network is employed, as LSTMs are specifically engineered for sequential data by incorporating internal memory states and gating mechanisms to learn long-term temporal dependencies.[17,19] The overall model structure is illustrated in Fig. 2.

To incorporate temporal context, a sliding-window representation is adopted. The input sequence at time step t is defined as

$$x_t = \left[\Delta R_{t-w+1}, \Delta R_{t-w+2}, \ldots, \Delta R_t\right], \tag{1}$$

where w denotes the window size. In this study, w = 50, corresponding to 0.5 s of historical context at a sampling frequency of 100 Hz. This context is essential for resolving the multivalued mapping associated with viscoelastic relaxation.[13] The internal operations of each LSTM unit are defined by the following series of gating mechanisms.[8,19]

Forget gate:

$$f_t = \sigma\left(W_f[h_{t-1}, x_t] + b_f\right) \tag{2}$$

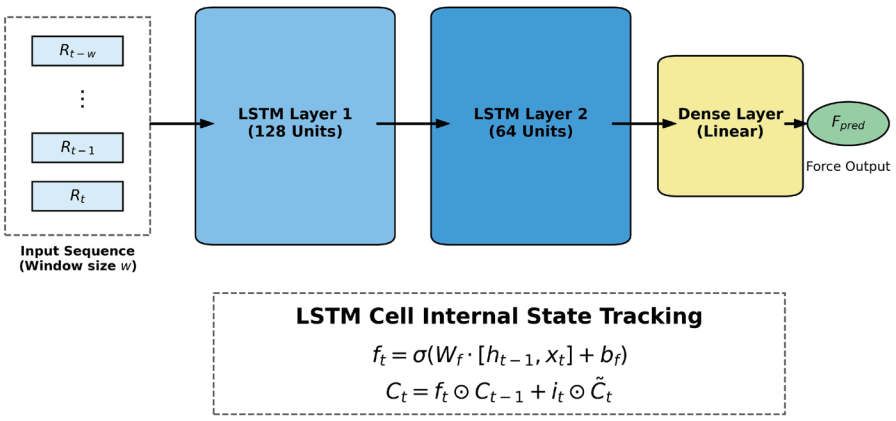

Fig. 2. (Color online) Stacked LSTM architecture with sliding-window input and regression output layer. The network input is the windowed sequence of the resistance variation ΔR only; the applied force is the regression target (output) and is not fed back as an input, and the actuator displacement is likewise not used as an input.

Input gate:

$$i_t = \sigma\left(W_i[h_{t-1}, x_t] + b_i\right) \tag{3}$$

Candidate cell state:

$$\tilde{C}_t = \tanh\left(W_C[h_{t-1}, x_t] + b_C\right) \tag{4}$$

Cell state update:

$$C_t = f_t \odot C_{t-1} + i_t \odot \tilde{C}_t \tag{5}$$

Output gate:

$$o_t = \sigma\left(W_o[h_{t-1}, x_t] + b_o\right) \tag{6}$$

Hidden state:

$$h_t = o_t \odot \tanh(C_t) \tag{7}$$

In Eqs. (2)–(7), $\sigma(\cdot)$ denotes the logistic sigmoid activation, tanh(·) the hyperbolic tangent activation, and $\odot$ the Hadamard (element-wise) product operator. At time step t, x_t is the input vector and h_{t-1} the hidden state inherited from the previous step. The forget, input, and output gates f_t, i_t, and o_t [Eqs. (2), (3), and (6)] regulate, respectively, how much of the previous cell state is retained, how much new information is written, and how much of the updated cell state is exposed as output. The terms W_f, W_i, W_c, and W_o are the corresponding weight matrices and b_f, b_i, b_c, and b_o the bias vectors of the forget gate, input gate, candidate cell state, and output gate, respectively; together they constitute the trainable parameters learned during optimization. The candidate cell state $\tilde{C}_t$ [Eq. (4)] proposes new content; the cell state $\tilde{C}_t$ [Eq. (5)] is updated as the element-wise ($\odot$) combination of the retained and the newly written information; and the hidden state h_t [Eq. (7)] is the gated output passed both to the next time step and, in the stacked configuration, to the upper LSTM layer. Together, Eqs. (2)–(7) define the recurrence executed inside every LSTM unit of the network, enabling it to selectively store and discard the deformation-history information that governs the hysteretic response.

By stacking two LSTM layers, the network can learn hierarchical temporal features.[16,17] The first layer extracts low-level signal fluctuations, whereas the second layer models higher-level abstractions related to the memory of past loading cycles.[11] The final force prediction is obtained through a fully connected regression layer:

$$\hat{F}_t = W_y \cdot h_t^{(2)} + b_y. \tag{8}$$

The optimized hyperparameters and training configuration of the model are summarized in Table 2.

2.4 Training strategy and implementation details

The optimization of model parameters was conducted by minimizing the mean squared error (E_{MSE}) objective function, which quantifies the discrepancy between the reference force and the network's predictions.[17]

The loss function is formulated as

$$E_{MSE} = \frac{1}{N}\sum_{i=1}^{N}(F_{ref,i} - \hat{F}_i)^2, \tag{9}$$

where N denotes the total number of samples within a training batch, whereas $F_{ref,i}$ and $\hat{F}_i$ represent the ground-truth and estimated force values, respectively. To navigate the complex, nonconvex loss surface associated with recurrent architectures, ADAM optimizer was employed.[20] Adam is particularly effective for tactile sensor data as it computes adaptive learning rates for individual parameters, facilitating stable convergence in the presence of the nonstationary and noisy gradients inherent in temporal sensing signals.[16,20]

Table 2
Hyperparameters and training configuration of proposed LSTM model.

Category	Hyperparameter	Symbol	Value	Description
Input	Window size	w	50	Temporal context (0.5 s at 100 Hz)
	Input feature	—	ΔR	Resistance variation
Architecture	Number of LSTM layers	—	2	Stacked architecture
	Hidden units (Layer 1)	—	128	Feature extraction
	Hidden units (Layer 2)	—	64	Feature compression
	Output layer	—	Dense[10]	Force regression
Training	Loss function	—	E_{MSE}	Mean squared error
	Optimizer	—	Adam	Adaptive optimization[4]
	Learning rate	η	1×10^{-3}	Initial learning rate
	Batch size	B	64	Mini-batch training
	Max epochs	—	200	Training limit
	Early stopping	—	Enabled	Based on validation loss
Regularization	Dropout rate	p	0.2	Prevent overfitting
Data Processing	Normalization	—	Z-score	Zero mean, unit variance
	Train/Test split	—	80/20	Dataset partition

The training process was executed with an initial learning rate of $\eta = 10^{-3}$ and a mini-batch size of $B = 64$ for a maximum of 200 epochs. To ensure the model generalizes effectively to unseen dynamic conditions and avoids the "catastrophic forgetting" of historical patterns, a systematic regularization strategy was implemented.[11,19] This included the integration of dropout layers ($p = 0.2$) between the stacked LSTM hidden states and the application of an early stopping mechanism, which halted training if the validation loss failed to improve for 15 consecutive epochs.[4,17] The model was implemented in Python using the Keras API on a TensorFlow backend, with NumPy and pandas for data handling and scikit-learn for the *Z*-score scaling and the computation of the error metrics.

The experimental dataset was partitioned into training and testing subsets using an 80:20 ratio to ensure rigorous validation.[16] Prior to training, all input features were subjected to Z-score normalization to map the raw resistance variations into a standardized distribution:

$$x_{norm} = \frac{x - \mu}{\sigma}, \tag{10}$$

where μ and σ are the mean and standard deviation of the training data. This preprocessing step is critical for preventing gradient saturation in the LSTM's activation functions and accelerating the overall optimization process. Concretely, the standardization is applied independently to each variable using statistics computed on the training set only: the input resistance variation is scaled as $R_{i,norm} = (R_i - \mu_R)/\sigma_R$, and the reference force used as the regression label is scaled analogously as $F_{i,norm} = (F_i - \mu_F)/\sigma_F$; predictions are mapped back to physical force units by the inverse transform before all errors are reported.[19,20] The optimized configuration ensures that the model can reliably resolve the rate-dependent signatures of the CNT–PDMS composite across the entire testing spectrum.

2.5 Performance evaluation metrics

The performance of the proposed model was evaluated using three standard regression metrics: E_{MAE}, root mean square error (E_{RMSE}), and the coefficient of determination (R^2).[16,17] These metrics provide complementary evaluation criteria: E_{MAE} reflects the average absolute deviation, E_{RMSE} penalizes larger errors more strongly, and R^2 quantifies the goodness of fit between predicted and reference signals.[8, 20]

E_{MAE} is defined as

$$E_{MAE} = \frac{1}{N}\sum_{i=1}^{N} |F_{ref,i} - \hat{F}_i|. \tag{11}$$

E_{RMSE} is given by

$$E_{RMSE} = \sqrt{\frac{1}{N}\sum_{i=1}^{N}(F_{ref,i} - \hat{F}_i)^2}. \tag{12}$$

R^2 is defined as

$$R^2 = 1 - \frac{\sum_{i=1}^{N}(F_{ref,i} - \hat{F}_i)^2}{\sum_{i=1}^{N}(F_{ref,i} - \bar{F}_{ref})^2}. \tag{13}$$

N denotes the number of samples, $F_{ref,i}$ and $\hat{F}_i$ represent the reference and predicted force for the i-th sample, respectively, and $\bar{F}_{ref}$ represents the mean value of the reference force. This comprehensive set of metrics ensures that the model's ability to resolve the path-dependent and rate-dependent signatures of the CNT–PDMS composite is accurately quantified.[4,8]

3. Results and discussion

3.1 Characterization of hysteresis behavior

To establish a quantitative baseline for evaluating the proposed compensation framework, the intrinsic electromechanical response of the CNT–PDMS soft sensor was first characterized under cyclic compressive loading.[8,18]

As shown in Fig. 3(a), the resistance response does not follow the applied force instantaneously. Instead, a noticeable phase lag is observed between the input force (F) and the corresponding resistance variation (ΔR). This temporal mismatch indicates that the sensor output is not merely a function of the current input but is deeply affected by its recent deformation history.[10,12] Such behavior is a hallmark of viscoelastic materials, where internal stress relaxation and entropic changes in the polymer chains occur over a finite time scale.[3,13]

When the same data are represented in the force–resistance domain, as illustrated in Fig. 3(b), a pronounced and asymmetric hysteresis loop is observed. This loop demonstrates the path-dependent nature of the sensor response: for a given resistance value, multiple force values exist depending on whether the sensor is undergoing loading or unloading.[14,15]

From a physical perspective, this behavior arises from the coupled effects of polymer viscoelasticity and the dynamic reconfiguration of conductive pathways within the MWCNT network.[3,8] Mechanical deformation alters the intertube distance, affecting both contact resistance and electron tunneling mechanisms.[9] During the loading and unloading cycles, the conductive network follows distinct evolution paths owing to internal friction and the sliding of nanotubes, leading to significant energy dissipation and the observed hysteresis.[11,12]

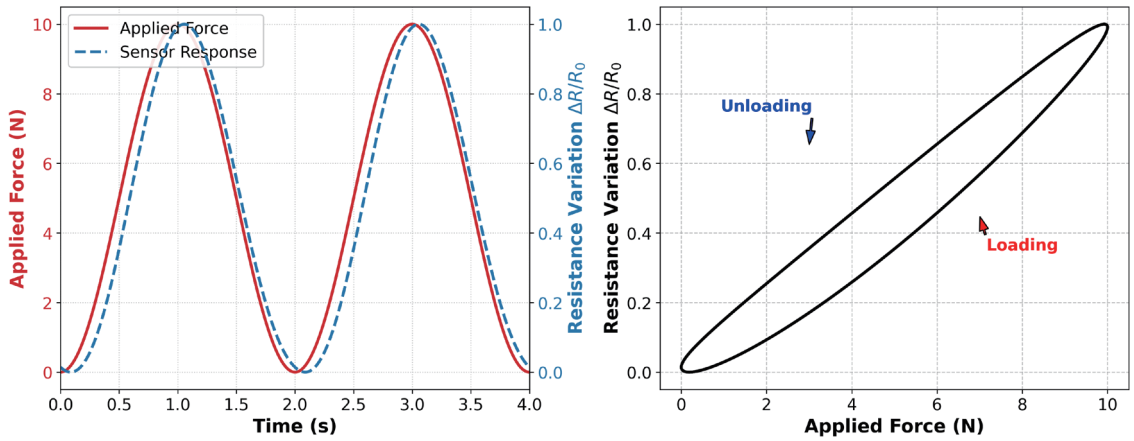

(a) (b)

Fig. 3. (Color online) Experimental characterization of hysteresis: (a) time-domain response and (b) force–resistance hysteresis loop.

Quantitatively, the maximum hysteresis error—defined as the maximum vertical gap in force between the loading and unloading branches of the hysteresis loop, normalized by the full-scale (maximum applied) force—was measured at 12.4% of the full-scale output. This significant deviation underscores the fundamental limitation of conventional static calibration approaches, which assume a unique one-to-one mapping between resistance and force.[2,10] Consequently, achieving accurate force reconstruction in soft robotic systems requires advanced modeling architectures that can incorporate temporal context to resolve the ambiguity inherent in these hysteretic responses.[16,19]

3.2 LSTM-based compensation and response linearization

To address the path-dependent nature of the sensor response, the proposed stacked LSTM model was trained to reconstruct the applied force from the temporal sequence of resistance measurements.[17,19] Because the actuator is displacement-controlled, the training data were generated by commanding sinusoidal compressive displacement profiles of the form $d(t) = d_0[1 - \cos(2\pi ft)]/2$, applied to the sensor surface; the resulting compressive force, which depends on the sensor stiffness and rate-dependent response, was recorded by the load cell and used as the ground-truth label. To expose the network to a broad range of dynamic conditions, the displacement amplitude d_0 was varied to span the full force range of approximately [0–F_{max}] N, and the excitation frequency f was varied over the set {0.1, 0.5, 1.0, 2.0} Hz. Cycles from all amplitudes and frequencies were pooled before the 80:20 split, so that the training and test subsets each contain examples drawn from every loading condition. The compensation results are visualized in Fig. 4.

As shown in Fig. 4(a), the predicted force ($\hat{F}$) closely follows the reference signal (F_{ref}) across multiple loading cycles. The model maintains high tracking accuracy during both the compression and relaxation phases, indicating that it successfully captures the complex temporal dependencies and phase lags inherent in the hysteretic response.[4,5]

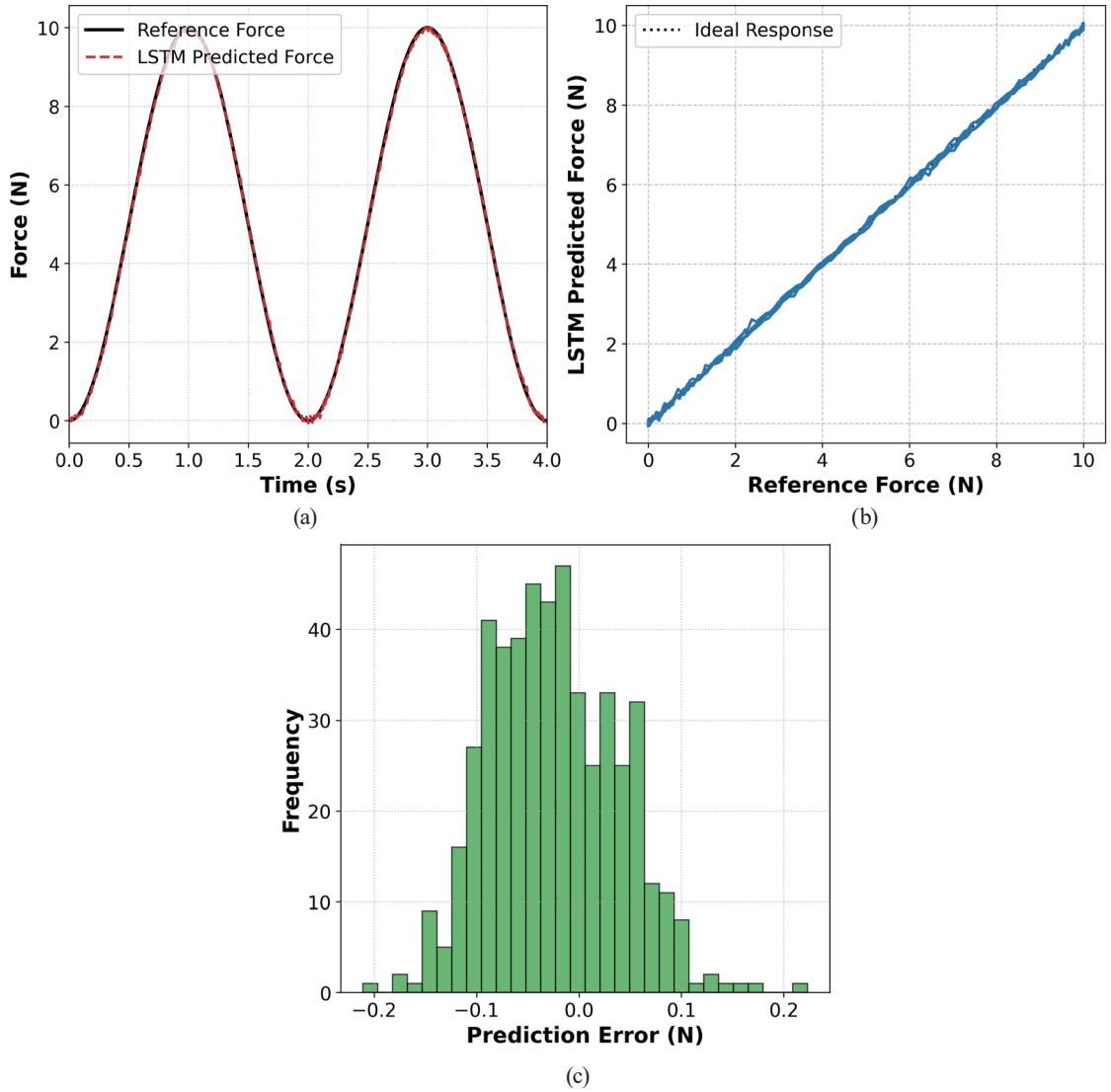

Fig. 4. (Color online) LSTM-based compensation results: (a) real-time tracking of force, (b) linearized force–resistance relationship after compensation, and (c) prediction error distribution

A more detailed observation of the linearization effect is presented in Fig. 4(b). After compensation, the previously wide and multivalued hysteresis loop of the uncompensated sensor (Fig. 3(b)) collapses into a near-linear relationship between resistance and force. This transformation demonstrates that the proposed framework effectively resolves the mapping ambiguity by incorporating historical deformation context, resulting in an approximately one-to-one correspondence between the electrical signal and the physical input.[14,17]

From a modeling perspective, this significant improvement can be directly attributed to the internal memory mechanism of the stacked LSTM architecture.[17,19] By processing continuous sequences of past inputs through a sliding-window strategy, the model implicitly encodes the instantaneous state of the CNT–PDMS composite, including its viscoelastic relaxation and the cumulative reconfiguration of the conductive filler network.[12,13] This enables the network to

distinguish between loading and unloading trajectories that are otherwise indistinguishable in static input–output mappings. In contrast, feed-forward architectures such as MLPs lack this temporal awareness and treat each measurement as an independent event, leading to irreducible residual hysteresis.[11,16]

The prediction error distribution shown in Fig. 4(c) remains tightly bounded within approximately ±0.1 N, following a Gaussian-like profile centered near zero. Quantitatively, the proposed framework achieves an E_{MAE} of 0.086 N, an E_{RMSE} of 0.134 N, and an R^2 of 0.988. Most importantly, the maximum hysteresis error is reduced from 12.4 to 1.8% of the full-scale output.[18] These results indicate that temporal deep learning transforms a path-dependent nonlinear response into a predictable and linearized mapping, significantly enhancing force estimation reliability.[2,4]

3.3 Comparative analysis with baseline models

To rigorously assess the effectiveness of the proposed architecture, the stacked LSTM model was compared against several baseline methods, including linear regression, polynomial regression, an MLP, and a gated recurrent unit (GRU) model.[16,17] The quantitative performance metrics are summarized in Table 3.

The results reveal a significant disparity between static and temporal modeling approaches. Linear and polynomial models exhibit the largest errors, as they assume a unique, single-valued mapping that cannot resolve the path-dependence inherent in viscoelastic materials.[14,15] While the MLP improves performance by capturing global nonlinearities,[16] it treats measurements as independent events.[17] Without an internal memory mechanism to store historical deformation states, the MLP essentially averages the loading and unloading branches of the hysteresis loop, leading to substantial residual errors.[11]

In contrast, recurrent architectures (GRU and LSTM) provide a substantial reduction in error by explicitly modeling the evolution of the sensor state over time. Among the temporal models, the proposed LSTM achieves the highest precision across all metrics. This superiority is attributed to the LSTM's gating architecture, specifically the "forget gate",[19] which allows the network to effectively maintain and update information regarding long-term viscoelastic relaxation times and cumulative filler network shifts.[12,13] Although the GRU also incorporates gating mechanisms, the more expressive structure of the LSTM provides a consistent advantage in modeling the complex, asymmetric memory effects of the CNT–PDMS system.[5,8]

Table 3
Performances of different models for hysteresis compensation.

Model	E_{MAE} (N)	E_{RMSE} (N)	R^2	Max error (%)	Inference time (ms)
Linear regression	0.742	0.915	0.764	14.8	0.5
Polynomial (3rd order)	0.521	0.684	0.825	11.2	0.8
MLP	0.315	0.428	0.882	8.5	2.1
GRU (1 layer)	0.112	0.165	0.965	3.1	10.4
Proposed LSTM	0.086	0.134	0.988	1.8	14.8

While the LSTM model incurs a higher computational cost, with an inference time of 14.8 ms, this latency remains well within the operational requirements for real-time robotic control and high-frequency tactile perception.[2,4,10] These findings confirm that hysteresis compensation in soft sensors is fundamentally a temporal inference problem rather than a static regression task.

3.4 Robustness under rate-dependent conditions

In practical applications, soft tactile sensors are subject to varying loading velocities, which significantly alter their electromechanical response and hysteresis area.[2,18] To evaluate the robustness and generalizability of the proposed framework, experiments were conducted over a wide frequency spectrum ranging from 0.1 to 2.0 Hz.

As illustrated in Fig. 5(a), both E_{MAE} and E_{RMSE} exhibit a gradual increase with the excitation frequency. This trend reflects the rate-dependent viscoelastic behavior of the PDMS matrix, where higher deformation rates reduce the time available for internal stress relaxation, thereby intensifying the hysteretic signatures.[10,12,13] It should also be noted that the sampling rate was held constant at 100 Hz across all tests, so that the number of samples acquired per loading cycle decreases as the excitation frequency rises (from about 1000 points per cycle at 0.1 Hz to about 50 points per cycle at 2.0 Hz). Part of the observed increase in E_{MAE} and E_{RMSE} may therefore stem from this coarser temporal resolution, which reduces the number of points available to the sliding window and can degrade fit quality, rather than from the viscoelastic mechanism alone. We further emphasize that a single model was trained on the pooled multifrequency dataset and then applied unchanged to all frequencies, including the higher-frequency tests; no separate model was trained per frequency. Despite this increase, the overall performance degradation remains moderate. Even at the highest frequency of 2.0 Hz, the model maintains an R^2 above 0.975, indicating that the learned temporal representations generalize effectively across diverse dynamic conditions.[4,15]

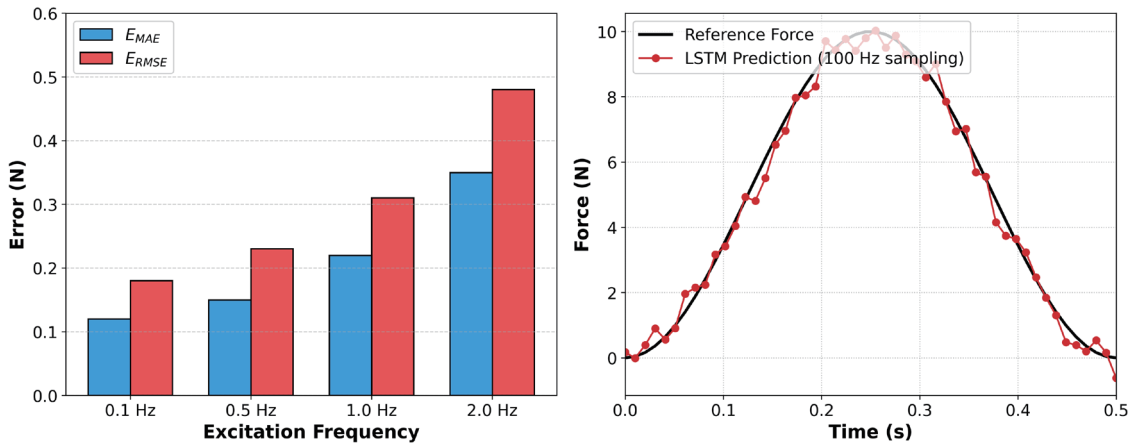

(a) (b)

Fig. 5. (Color online) Robustness analysis. (a) Variation of error metrics with loading frequency. (b) Distribution of prediction error.

Table 4
Performance of proposed model under different loading frequencies.

Frequency (Hz)	E_{MAE} (N)	E_{RMSE} (N)	R^2	Max error (%)
0.1	0.052	0.078	0.992	1.1
0.5	0.086	0.134	0.988	1.8
1.0	0.098	0.155	0.984	2.2
2.0	0.142	0.198	0.975	3.1
Mean	0.095	0.141	0.985	2.05

The prediction error distribution shown in Fig. 5(b) follows an approximately Gaussian profile centered near zero, which suggests that the model does not introduce systematic bias or cumulative drift across frequencies. The remaining discrepancies can be primarily attributed to stochastic variations in the filler network and high-frequency measurement noise.[9,11] The detailed quantitative results are summarized in Table 4.

Overall, these results demonstrate that the stacked LSTM framework is capable of capturing both nonlinear hysteresis behavior and its rate-dependent characteristics.[4] This stability indicates that the model not only improves accuracy under specific conditions but also maintains reliable performance across a range of operating regimes relevant to real-time soft robotic and medical applications.[6,10]

4. Conclusions

In this study, we demonstrated a robust temporal deep learning framework based on stacked LSTM networks for the precise mitigation of nonlinear hysteresis in CNT–PDMS soft tactile sensors.[4,19] By formulating hysteresis compensation as a temporal inference problem rather than a conventional memoryless regression task, the proposed architecture successfully decoded the complex deformation history inherent in viscoelastic nanocomposites.[12,13] The integration of a sliding-window strategy with hierarchical feature representation effectively resolved the multivalued mapping between electrical resistance and applied force, transforming a path-dependent response into a linearized and predictable output.[16,17]

Quantitative results revealed a substantial reduction in maximum hysteresis error, decreasing from 12.4 to 1.8% of the full-scale output, while maintaining a high R^2 of 0.988. Furthermore, the model's ability to sustain stable performance across a broad frequency spectrum (0.1–2.0 Hz) underscores its generalizability to the dynamic conditions typical of soft robotic interactions.[8,18] These findings suggest that recurrent neural networks provide a superior paradigm for the calibration of intelligent e-skins, bridging the gap between raw material behavior and high-fidelity tactile perception.[2,4]

Despite these promising outcomes, certain challenges remain regarding the translation of this technology to practical applications.[2] The current investigation focused on a single sensor configuration; thus, future efforts must address long-term performance degradation due to structural fatigue and environmental sensitivities such as temperature-induced drift. It should also be emphasized that the present scheme was validated only for pulsating compressive forces of constant frequency; its performance under variable-frequency or arbitrary nonperiodic

loading was not tested here and remains to be investigated.[11,13] In addition, the computational intensity of stacked LSTM architectures necessitates the development of lightweight or quantized models for deployment on resource-constrained embedded systems at the edge.[20]

Future research will focus on extending this temporal framework to large-scale, multimodal sensor arrays capable of simultaneous force and temperature discrimination.[1,18] The integration of physics-informed constraints into the deep learning architecture also represents a promising direction for improving model interpretability and reduce training data requirements.[10,12] Ultimately, these advancements will facilitate the development of a new generation of tactile-intelligent systems for surgical robotics, neuroprosthetics, and collaborative human–machine interfaces.[3,6]

Acknowledgments

The author would like to express his sincere gratitude to the research facilities and technical support staff for providing the necessary equipment and assistance during the fabrication and characterization of the CNT-PDMS nanocomposites. Special thanks are extended to colleagues and academic peers for their insightful discussions and constructive feedback regarding the implementation of the temporal deep learning framework. Their contributions have significantly enhanced the clarity and scientific rigor of this work.

References

1 E. Donato, E. Falotico, and T. G. Thuruthel: Proc. 2024 IEEE 7th Int. Conf. Soft Robotics (RoboSoft) (IEEE, 2024) 311. https://doi.org/10.1109/RoboSoft60065.2024.10522007
2 Z. Yao, W. Wu, F. Gao, M. Gong, L. Zhang, D. Wang, B. Guo, L. Zhang, and X. Lin: Nano-Micro Lett. **18** (2026) 37. https://doi.org/10.1007/s40820-025-01872-4
3 M. L. Hammock, A. Chortos, B. C.-K. Tee, J. B.-H. Tok, and Z. Bao: Adv. Mater. **25** (2013) 5997. https://doi.org/10.1002/adma.201302240
4 Q. Nie, F. Wang, F.-S. Yang, H. Xun, J. Hou, Q. Xu, Y. Hong, J. Zhang, X. Wei, Y.-F. Lin, P.-W. Chiu, L. Zeng, M. Li, B. Wang, and J. Zhang: Adv. Mater. **38** (2026). https://doi.org/10.1002/adma.202510646
5 S. Choi, S. I. Han, D. Kim, T. Hyeon, and D.-H. Kim: Chem. Soc. Rev. **48** (2019) 1566. https://doi.org/10.1039/C8CS00706C
6 M. Amjadi, K.-U. Kyung, I. Park, and M. Sitti: Adv. Funct. Mater. **26** (2016) 1678. https://doi.org/10.1002/adfm.201504755
7 J.-S. Kim and G.-W. Kim: Sensors **17** (2017) 229. https://doi.org/10.3390/s17020229
8 Y. He, X. Lu, D. Wu, M. Zhou, G. He, J. Zhang, L. Zhang, H. Liu, and C. Liu: Sens. Actuators, A **358** (2023) 114408. https://doi.org/10.1016/j.sna.2023.114408
9 J. Park, Y. Lee, J. Hong, M. Ha, Y.-D. Jung, H. Lim, S. Y. Kim, and H. Ko: ACS Nano **8** (2014) 4689. https://doi.org/10.1021/nn500441k
10 J. de la Morena, F. Ramos, and A. S. Vázquez: Actuators **14** (2025) 321. https://doi.org/10.3390/act14070321
11 Z. Wang, T. Zhang, L. Zhang, X. Wang, Y. Yao, Q. Liu, Y. Liu, and D. Chen: Micromachines **17** (2026) 496. https://doi.org/10.3390/mi17040496
12 J. Zou and G. Gu: Polymers **10** (2018) 525. https://doi.org/10.3390/polym10050525
13 R. Ariati, F. Sales, A. Souza, R. A. Lima, and J. Ribeiro: Polymers **13** (2021) 4258. https://doi.org/10.3390/polym13234258
14 G. Abdul-Hussain, W. Holderbaum, T. Theodoridis, and G. Wei: Sensors **23** (2023) 7293. https://doi.org/10.3390/s23167293
15 X. Shan, H. Song, H. Cao, L. Zhang, X. Zhao, and J. Fan: Sensors **21** (2021) 269. https://doi.org/10.3390/s21010269

16 C. Xie, R. Yao, L. Zhu, H. Gong, H. Li, and X. Chen: Ind. Eng. Chem. Res. **62** (2023) 519. https://doi.org/10.1021/acs.iecr.2c03137
17 J. Zheng, L. Ma, Y. Wu, L. Ye, and F. Shen: ACS Omega **7** (2022) 16653. https://doi.org/10.1021/acsomega.2c01108
18 A. H. CP, S. K. Pillai, S. Naskar, T. Mondal, and K. Naskar: ACS Appl. Mater. Interfaces **16** (2024) 48211. https://doi.org/10.1021/acsami.4c07163
19 S. Hochreiter and J. Schmidhuber: Neural Comput. **9** (1997) 1735. https://doi.org/10.1162/neco.1997.9.8.1735
20 D. P. Kingma and J. Ba: Proc. Int. Conf. Learn. Represent. (ICLR) (2015). https://doi.org/10.48550/arXiv.1412.6980